ISSN (Print) 1226-1750
ISSN (Online) 2233-6656
Journal of Magnetics 24(3), 423-428 (2019) https://doi.org/10.4283/JMAG.2019.24.3.423

Magnetic Flux Leakage Image Enhancement using Bidimensional Empirical Mode Decomposition with Wavelet Transform Method in Oil Pipeline Nondestructive Evaluation

Liang Chen[1], Jingcheng Li[2], Yakai Zeng[1], Yongqiang Chen[1], and Wei Liang[1]*

[1]*School of Mechanical and Electrical Engineering, University of Electronic Science and Technology of China, Chengdu 611731, China*
[2]*School of Resources and Environment, University of Electronic Science and Technology of China, Chengdu 611731, China*

(Received 17 October 2018, Received in final form 21 June 2019, Accepted 10 July 2019)

The magnetic flux leakage (MFL) method is the most widely used and cost-effective inspection technique for oil pipeline. However, noise is inevitable in the process of data collection; thus, the image enhancement method can be more intuitive to identify the defects in an oil pipeline MFL inspection. In this paper, the bidimensional empirical mode decomposition (BEMD) method has been used to study oil pipeline MFL images. The MFL image is decomposed into a finite number of two-dimensional intrinsic mode functions (BIMF) and a residual component by the BEMD. The wavelet transform (WT) was used to remove the noise in the BIMF. The image was then reconstructed by retaining the basic information and removing the noise. The results show that the noise is effectively removed and the detail of the MFL image is well preserved. Thus, the BEMD with WT method for oil pipeline MFL image enhancement is better than the mean filtering method and the WT method.

Keywords : magnetic flux leakage, nondestructive evaluation, image enhancement, bidimensional empirical mode decomposition, oil pipeline

1. Introduction

Over the years, many different nondestructive testing (NDT) techniques have been investigated for evaluating the condition of pipelines [1-4]. Magnetic flux leakage (MFL) method is a widely used NDT technique to measure and locate corrosion in oil and gas pipelines [5-7]. In this technique, the wall of the pipeline is magnetised axially to near saturation flux density. If, at some point, the wall thickness is reduced by a defect, a higher fraction of the magnetic flux will 'leak' from the wall into the air inside and outside the pipe [8]. This MFL can be detected by a Hall probe or an induction coil and stored in a computer for analysis [9].

When we reconstruct the MFL data into 2D defect profile image, the defect analysis efficiency and reliability are improved. Unfortunately, the MFL data are usually contaminated by various noise sources. Mandayam used wavelet basis functions to provide selective invariant features and eliminate image intensity variations from undesirable changes [10]. Daniel selected the appropriate wavelet denoising technique for filtering the MFL data [11].

Bidimensional empirical mode decomposition (BEMD) [12] is an auto-adaptive method for analysis of nonlinear or non-stationary signals and images which has been proven to be effective for some image processing tasks [13, 14].

In this paper, the BEMD method has been used to study oil pipeline MFL images. The paper is organized as follows. In section 2, we will introduce the basic concept and algorithm of BEMD method, The MFL image enhancement using BEMD with wavelet transform (WT) is given in section 3. In section 4, we summarize the results of the study and draw conclusions.

2. The Bidimensional Empirical Mode Decomposition

The bidimensional empirical mode decomposition (BEMD) is the 2D extension of the empirical mode decomposition (EMD), which is part of the Hilbert-Huang transform (HHT) developed by Huang *et al.* [15, 16]. This decomposition technique is adaptive and appears to be a suitable for nonlinear, non-stationary data analysis.

*Corresponding author: Tel: +86-137-3085-0603
Fax: +86-28-6183-0227, e-mail: liangwei@uestc.edu.cn

This decomposition is developed from the simple assumption that any image data consist of different simple intrinsic modes of oscillations. Its principle is to decompose adaptively a given signal into amplitude- and frequency-modulation (AM-FM) components or into a two-dimensional intrinsic mode function (BIMF). Each BIMF has the same number of zero crossings and extrema (minus one) and each BIMF is symmetric with respect to a zero mean. Each mode which extracts locally the highest frequency oscillations out of original signal is called a 'sifting process'. A 2D sifting process can be summarized as follows: [17, 18]

(1) Initialization: $r_0(m, n) = I(m, n)$, $k = 1$, $(m, n) \in [0, M-1] \times [0, N-1]$, where M and N are the numbers of columns and rows of a discrete-domain image.

(2) Extraction of the kth IMF, $imf_k(m, n)$:

a) Initialization: $h_{k,0}(m, n) = r_{k-1}(m, n)$, $l = 1$.

b) Identify all the local maxima and local minima of $h_{k,l-1}(m, n)$.

c) Generate the upper and lower envelopes $e_{\max,l-1}(m, n)$ and $e_{\min,l-1}(m, n)$ by interpolating the maxima and minima points respectively.

d) For each local point (m, n), calculate the mean of the upper and lower envelopes.

$$e_{mean,l-1}(m,n) = \frac{e_{\max,l-1}(m,n) + e_{\min,l-1}(m,n)}{2}$$

e) $h_{k,l}(m, n) = h_{k,l-1}(m, n) - e_{mean,l-1}(m, n)$

f) If the stopping criterion is met, then $imf_k(m, n) = h_{k,l}(m, n)$; else, $l = l + 1$.

(3) $r_k(m,n) = r_{k-1}(m,n) - imf_k(m,n)$

(4) If $r_k(m, n)$ is monotonic, the sifting process is completed, otherwise, go to step 2.

The image can be finally expressed as the sum of the IMFs and the last residue:

$$I(m,n) = \sum_{k=1}^{K} imf_k(m,n) + r_k(m,n), k = 1, \cdots K \quad (1)$$

To stop the IMF extraction, the standard deviation (SD) computed from the two consecutive sifting results as:

$$SD = \sum_{m=0}^{M}\sum_{n=0}^{N}\left[\frac{\left|(h_{k,l-1}(m,n) - h_{k,l}(m,n))\right|^2}{h_{k,l-1}^2(m,n)}\right] \quad (2)$$

A typical value for the SD can be set between 0.02 and 0.3.

3. MFL Image Enhancement using BEMD with WT

The magnetic flux density is calculated for flaws by using the three-dimensional finite element method (FEM) [19]. Fig. 1 shows the geometry of the problem in a simplified 3D MFL model. The specimen length is 500 mm, width is 120 mm, and thickness is 12 mm. The magnetic circuit consists of the yoke, permanent magnet, brush and the pipeline. Two permanent magnets, of thickness 20 mm, are used for magnetic flux induction to magnetize the pipeline to saturation, and the material accumulates high magnetic energy, with high coercive force of 872000 A/m and stable magnetic property. The material of the pipeline is X52 and the yoke is mild steel. The flaw is located at the center of the specimen.

Figure 2 and Fig. 3 are the original images of the radial component (RC) and the axial component (AC) of the magnetic flux density in the vicinity of a flaw, which length is 10 mm, width is 10 mm, and depth is 8 mm, lift-off is 2 mm.

Figure 2 and Fig. 3 were corrupted by salt and pepper noise at 25 %, respectively. Figure 4 is an image of Fig. 2 after adding pepper noise at 25 %. The decomposition results are presented in Fig. 5, we get 6 IMFs and a residual component. The WT is applied to filter every

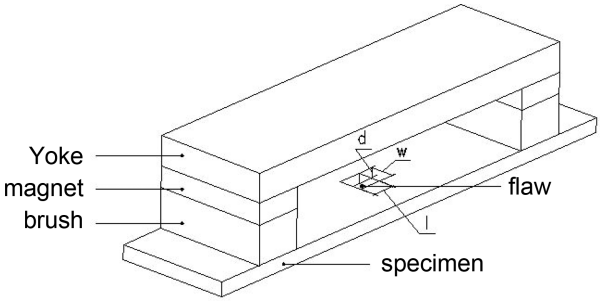

Fig. 1. Geometry of 3D MFL model.

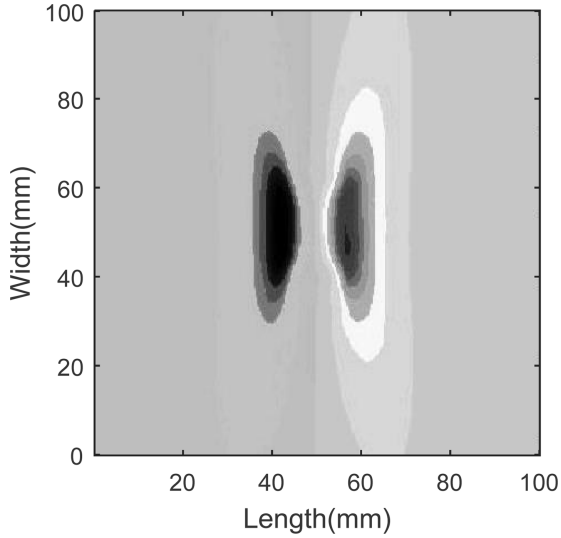

Fig. 2. Original Image of the RC by FEM.

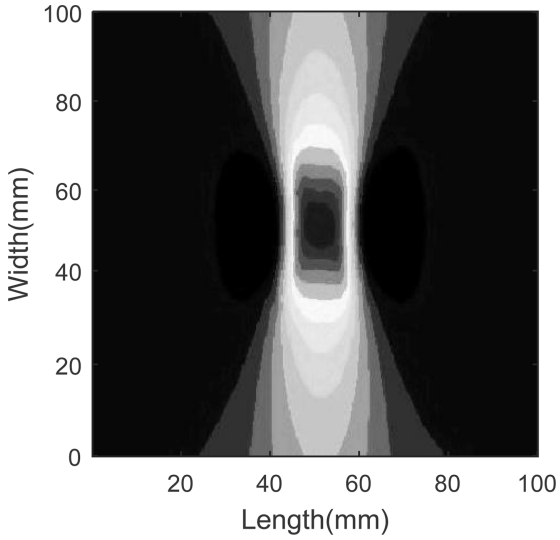

Fig. 3. Original Image of the AC by FEM.

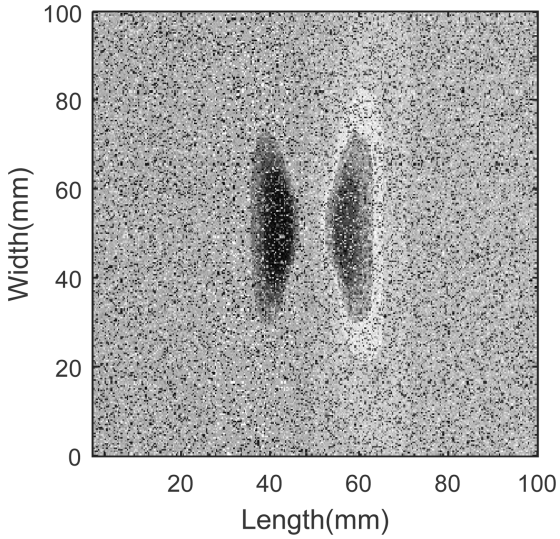

Fig. 4. Noisy Image of the RC by FEM with Salt & Pepper Noise.

IMF. The sum of all IMFs after filtering, added to the residual component reconstructs the original image. Figure 6 shows the reconstructed image of the RC. The reconstructed image of the AC is shown in Fig. 7.

At the same time, the MFL experiments were performed [19]. The apparatus contain a permanent magnet assembly, a DC motor control system, a data acquisition system (DAS) and other associated units. The permanent magnet assembly includes a magnetic circuit, a hall probe, and a signal pre-procession circuit. There are 16 Hall sensors of which lift-off is 2 mm to measure the leakage flux, with the necessary amplification and filter to record the signal.

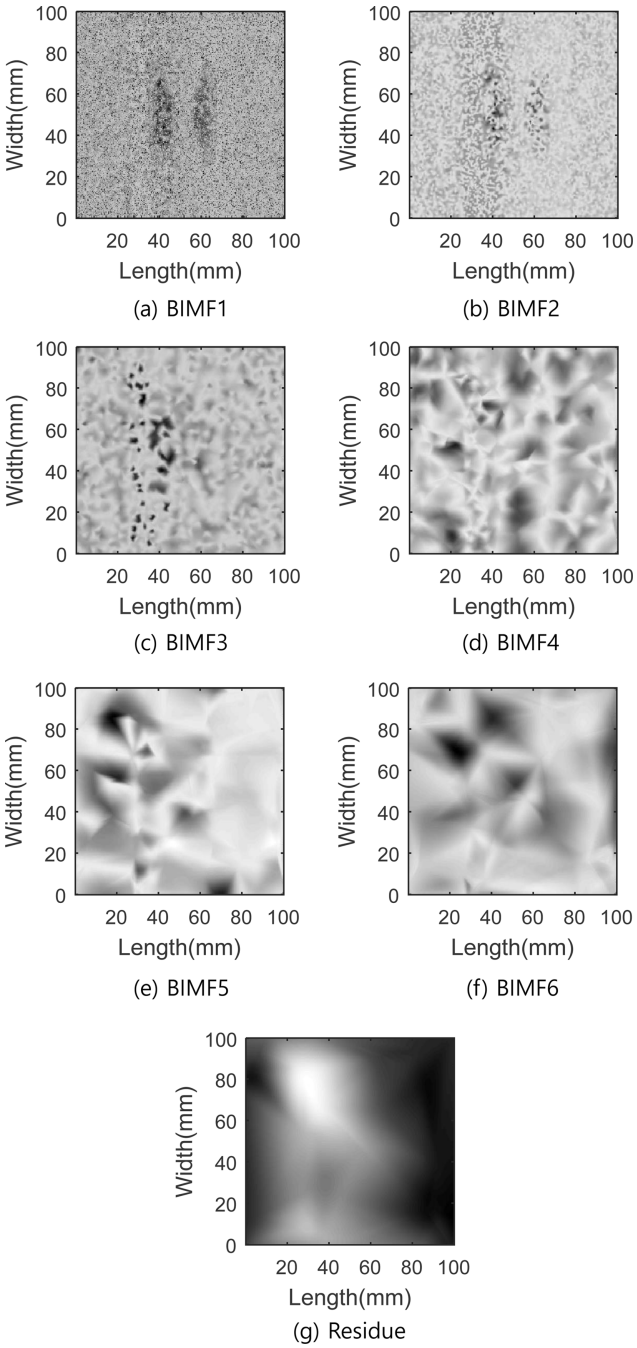

Fig. 5. Noisy image of the RC by FEM decomposition with BEMD.

The specimen thickness is 12 mm. Figure 8 and Fig. 9 are the original images of the RC and AC of magnetic flux density in the vicinity of a flaw, which length is 12 mm, width is 12 mm, and depth is 6 mm. Figure 10 and Fig. 11 are the reconstructed image of the RC and AC, respectively.

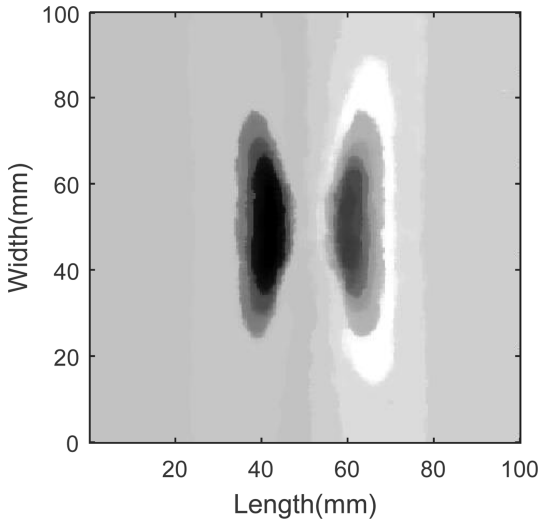

Fig. 6. Reconstructed Image of the RC by FEM.

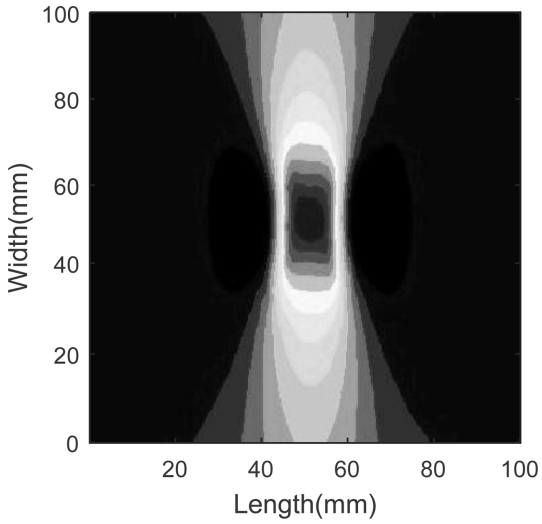

Fig. 7. Reconstructed Image of the AC by FEM.

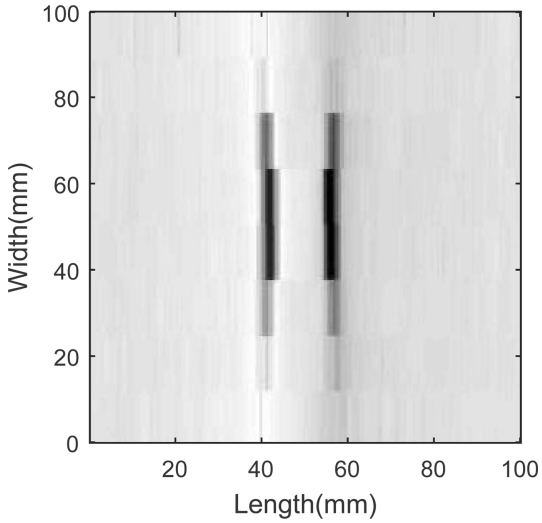

Fig. 8. Original Image of the RC by Experiment.

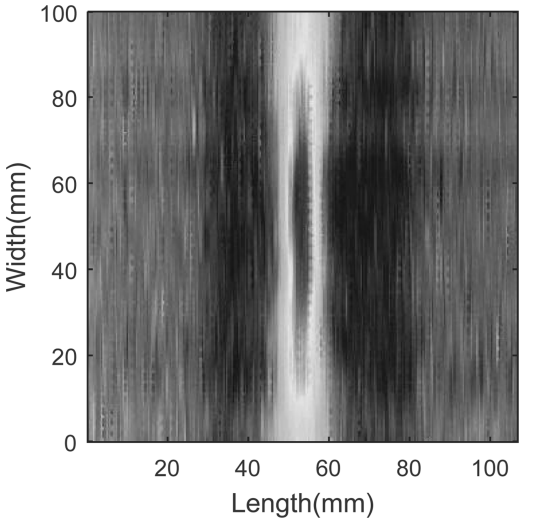

Fig. 9. Original Image of the AC by Experiment.

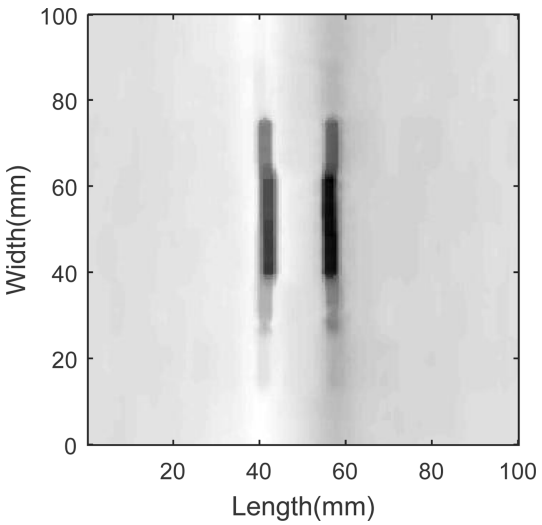

Fig. 10. Reconstructed Image of the RC by Experiment.

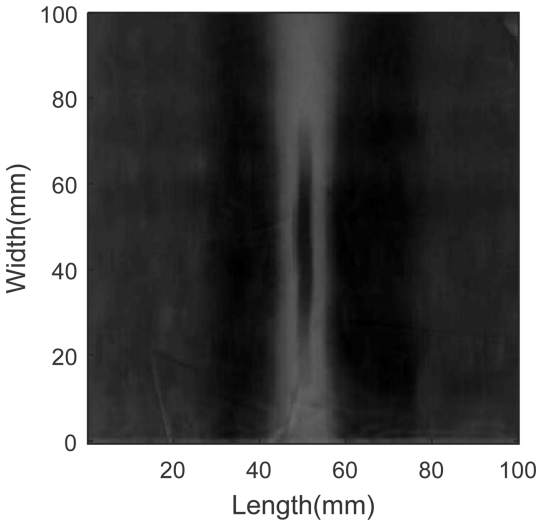

Fig. 11. Reconstructed Image of the AC by Experiment.

Table 1. MSE and PSNR values of the BEMD with WT method compared with MF and WT.

MFL Image	MF		WT		BEMD with WT	
	MSE	PSNR (dB)	MSE	PSNR (dB)	MSE	PSNR (dB)
AC with FEM	302.41	72.42	88.52	77.48	68.96	79.10
RC with FEM	241.98	71.46	75.63	76.79	52.03	77.88
AC with Experiment	213.79	25.16	155.77	26.42	107.56	28.60
RC with Experiment	198.37	24.83	148.39	26.21	89.75	27.81

4. Results and Discussion

4.1. Results

In section 3, the MFL image enhancement method, namely BEMD with WT, has been used in MFL images which include AC with FEM, RC with FEM, AC with Experiment and RC with Experiment. The execution of the proposed method is compared with mean filter (MF) and WT.

Mean square error (MSE) and peak signal-to-noise ratio (PSNR) are used to evaluate the quality of the reconstructed images, shown below as:

$$\mathrm{MSE} = \frac{\sum_{i=1}^{M}\sum_{j=1}^{N}\left[f(i,j)-\hat{f}(i,j)\right]^2}{M\times N} \tag{3}$$

$$\mathrm{PSNR} = 10\log_{10}\left(\frac{M\times N\times 255^2}{\sum_{i=1}^{M}\sum_{j=1}^{N}\left[\left[f(i,j)-\hat{f}(i,j)\right]^2\right]}\right) \tag{4}$$

$f(i,j)$ is the original image, and $\hat{f}(i,j)$ is the denoise image or reconstructed image. The size of the image is $M \times N$.

The execution results of the proposed method as compared with MF and WT is shown in Table 1.

4.2. Discussions

PSNR and MSE are the parameters that determine the quality of the image. MSE is characterized as a squared average of positive errors between unique input image and enhanced output image. MSE ought to be low for better enhanced image. Based on the MSE values, the PSNR can be calculated to ensure the enhancement of the output image.

For a good quality image, the PSNR value is maximum whereas the MSE is minimum. From Table 1, the proposed method produces higher PSNR value and minimum MSE values so that the proposed method of this paper produces the image with better quality compared to the other methods. The noise is effectively removed and the detail of the MFL image is well preserved.

5. Conclusions

We use the BEMD with the WT method to enhance MFL image in oil pipeline nondestructive evaluation. The MFL image is decomposed into a finite number of two-BIMF and a residual component by the BEMD, the WT was used to remove the noise in the BIMF. The image was then reconstructed by retaining the basic information and removing the noise. The analysis of the proposed method in terms of PSNR and MSE determines the effectiveness of the algorithm when compared with the other existing methods like MF and WT.

Acknowledgment

This work was supported by Postdoctoral Foundation of China (145067, 164836).

References

[1] W. Liang and L. Chen, J. Inst. **14**, 12001 (2009).
[2] L. Kang, C. Zhang, S. Dixon, H. Zhao, S. Hill, and M. H. Liu, NDT&E Int. **86**, 36 (2017).
[3] T. Azizzadeh and M. S. Safizadeh, J. Magn. **23**, 152 (2018).
[4] S. P. Song and Y. J. Ni, Chin. J. Mech. Eng. **31**, 81 (2018).
[5] L. Chen, X. Li, X. B. Li, and Z. Y. Huang, Rev. Sci. Instrum. **80**, 025105 (2009).
[6] Z. Y. Huang, P. W. Que, and L. Chen, NDT&E Int. **39**, 61 (2006).
[7] Y. Li, L. Udpa, and S. S Udpa, IEEE Trans. Magn. **40**, 410 (2004).
[8] X. B. Li, X. Li, L. Chen, P. F. Feng, H. D. Wang, and Z. Y. Huang, J. Mech. Sci. Technol. **23**, 1 (2009).
[9] T. Azizzadeh, M. S. Safizadeh, Measurement **138**, 5 (2019).
[10] S. Mandayam, L. Udpa, S. S. Udpa, and W. Lord, NDT&E Int. **30**, 297 (1997).
[11] J. Daniel, R. Mohanagayathri, and A. Abudhahir, International Conference on Electronics and Communication Systems, 1 (2014).
[12] J. C. Nunes, Y. Bouaoune, E. Delechelle, O. Niang, and Ph. Bunel, Image Vis. Comput. **21**, 1019 (2003).

[13] X. Q. Qin, G. Hu, and K. Hu, J. Electron. Imaging **27**, 013017 (2018).
[14] Y. H. Yang, Y. Li, and X. Y. Zhu, Acta Oceanol. Sin. **36**, 86 (2017).
[15] Q. Miao, D. Wang, and M. Pecht, J. Mech. Sci. Technol. **24**, 2421 (2010).
[16] J. C. Nunes, Y. Bouaoune, E. Delechelle, O. Niang, and P. Bunel, Image Vis. Comput. **21**, 1019 (2003).
[17] G. L. Xu, X. T. Wang, and X. G. Xu, Pattern Recogn. **42**, 718 (2009).
[18] L. L. He and H. Y. Wang, Proc. Int. Conf. Pattern Recognit. Hong Kong (2006) pp. 1196-1199.
[19] X. B. Li, X. Li, L. Chen, P. F. Feng, H. D. Wang, and Z. Y. Huang, J. Mech. Sci. Technol. **23**, 109 (2009).